JGR Solid Earth

RESEARCH ARTICLE
10.1029/2019JB018683

Low Friction Coefficient of Phyllosilicate Fault Gouges and the Effect of Humidity: Insights From a New Microphysical Model

S. A. M. den Hartog[1,2], D. R. Faulkner[1], and C. J. Spiers[3]

[1]Rock Deformation Laboratory, School of Environmental Sciences, University of Liverpool, Liverpool, UK, [2]Now at The Lyell Centre, Heriot-Watt University, Edinburgh, UK, [3]HPT Laboratory, Department of Earth Sciences, Faculty of Geosciences, Utrecht University, Utrecht, Netherlands

Key Points:
- We develop a cleavage-based model for 2:1 phyllosilicate (muscovite) friction
- The model predicts realistic trends in friction coefficient with humidity and velocity
- Absolute friction coefficient depends on poorly constrained atomic scale shear resistance highlighting the need for additional experiments

Supporting Information:
- Supporting Information S1

Correspondence to:
S. A. M. den Hartog,
s.den_hartog@hw.ac.uk

Citation:
den Hartog, S. A. M., Faulkner, D. R., & Spiers, C. J. (2020). Low friction coefficient of phyllosilicate fault gouges and the effect of humidity: Insights from a new microphysical model. *Journal of Geophysical Research: Solid Earth*, *125*, e2019JB018683. https://doi.org/10.1029/2019JB018683

Received 9 SEP 2019
Accepted 28 MAY 2020
Accepted article online 31 MAY 2020

Abstract Fault slip is often localized in phyllosilicate-rich fault gouges in a manner consistent with the relatively low friction coefficients measured for dry and especially wet phyllosilicates in laboratory experiments. However, the microphysics controlling these low friction coefficients remains unclear. Here, we propose a microphysical model, inspired by microstructural observations, for the prediction of the absolute value of the friction coefficient of pure dry and wet phyllosilicates. Experimentally produced phyllosilicate gouges suggest that shearing is controlled by sliding along (001) grain/platelet interfaces operating in series with removal of overlapping grain edge barriers by basal cleavage. We derive a model incorporating a subcritical crack propagation equation for the latter, constrained by subcritical crack growth data for muscovite. Model predictions for muscovite show similar trends regarding the effects of humidity and slip velocity on friction coefficient as do experiments at room temperature. The absolute value predicted for the friction coefficient is difficult to compare with experimental values, as it critically depends on atomic scale (001) sliding resistance, which is poorly constrained by available experimental data. Further discrepancies with experimental data can be explained by effects of varying grain size, grain aspect ratio, and porosity on the friction coefficient. While numerous qualitative explanations have been proposed previously for the low friction coefficient exhibited by phyllosilicates, especially in the presence of water, our study provides a new step toward a quantitative, physically based model.

1. Introduction

Phyllosilicate-rich fault zones are widespread in the Earth's crust, with the strands richest in phyllosilicates often accommodating the bulk of the shear strain, thus pointing to low shear strength compared with surrounding protolith material (e.g., Collettini et al., 2009; Holdsworth et al., 2011). This low strength has been confirmed by numerous experimental studies, which demonstrate friction coefficients for wet phyllosilicate gouges of typically 0.2 to 0.4 at upper crustal *P-T* conditions, compared with values of 0.3–0.8 in the dry state (e.g., Moore & Lockner, 2004) versus 0.6 to 0.85 for most other rock forming minerals tested wet and dry (e.g., Byerlee, 1978).

However, the physical processes controlling phyllosilicate friction and its dependence on sliding rate, temperature, normal stress, and composition remain unclear. The highly anisotropic cleavage and crystal plastic properties of phyllosilicates (Mares & Kronenberg, 1993), and the intense alignment of atomically flat, platy (001) crystallites observed in sheared phyllosilicate gouges (e.g., Den Hartog et al., 2012; Lu & He, 2014; Misra & Burg, 2012; Van Diggelen et al., 2010), mean that quantitative models explaining friction in terms of plastic spreading and shearing of asperities (e.g., Bar-Sinai et al., 2014; Dieterich & Kilgore, 1994) are unlikely to apply. Models describing friction in terms of isotropic (equi)granular flow accompanied by pressure solution (Chen & Spiers, 2016; Den Hartog & Spiers, 2014; Niemeijer & Spiers, 2007) are also inappropriate for pure phyllosilicate gouge. A widely accepted, qualitative explanation for low frictional strength is that by Morrow et al. (2000) and Moore and Lockner (2004), who used an observed correlation between electrostatic separation energy and friction coefficient to argue that dry shear occurs by breaking of the relatively weak (001) interlayer bonds of sheet structure minerals. In the wet case, they envisioned that shear occurs through water films at platelet surfaces, where the film-surface bond strength is assumed to be determined by the interlayer bond strength (Moore & Lockner, 2004; Morrow et al., 2000). Electrical

double layer and hydration forces related to the adsorbed water are repulsive, hereby reducing the friction coefficient (Sakuma, 2013). However, based on new calculations of the interlayer bonding energies, Sakuma and Suehara (2015; cf. Sakuma et al., 2018) cast doubt on the existence of a linear relation between the friction coefficient and interlayer bond strength and hence on the explanation of dry friction as the result of breaking of interlayer bonds. Note also that all previous explanations for frictional strength consider sliding interactions between atomically flat (001) platelets only and may not apply to gouges where the platelets are rough and other interactions between particles dominate.

Despite the numerous studies, extrapolation of laboratory-derived rate-and-state (Dieterich, 1978, 1979; Ruina, 1983) and plastic-asperity (Bar-Sinai et al., 2014) friction models for phyllosilicates, beyond laboratory conditions, is poorly constrained, as their assumed mechanistic basis has not been demonstrated. Such mechanistic constraints are important, as most friction data for pure phyllosilicate gouges have been obtained under quite limited experimental conditions, that is, at room temperature, normal stresses up to 100 MPa, and sliding rates in the range 1 to 100 μm/s, often with poorly known water content, relative humidity (RH), or pore pressure (Behnsen & Faulkner, 2012; Bos et al., 2000; Crawford et al., 2008; Faulkner et al., 2018; Ikari et al., 2011; Lu & He, 2014; Mares & Kronenberg, 1993; Mariani et al., 2006; Misra & Burg, 2012; Moore & Lockner, 2004; Morrow et al., 2000, 2017; Scruggs & Tullis, 1998; Shimamoto, 1986; Shimamoto & Logan, 1981).

Here, we take a first step in developing such a mechanistic model for phyllosilicate friction, based on processes recognized from microstructural observations. We apply the model to predict the friction coefficient of muscovite fault gouge at room temperature, including the effects of RH and shearing velocity. The model results obtained show trends in friction coefficient with RH and slip velocity similar to trends seen in available experimental data for muscovite and similar 2:1 phyllosilicates; they provide new insight into the effects of water on phyllosilicate friction and into possible causes of slip hardening seen in pure phyllosilicate. Absolute values of the coefficient of friction and the effect of the normal stress on the friction coefficient, however, are poorly reproduced, emphasizing the need for better constrained input parameters and the need to account for possible additional microphysical processes.

2. Model Development

Friction experiments on 1–2 mm thick layers of (near-)pure phyllosilicate gouge often show slip hardening behavior at a continuously decreasing rate (Den Hartog et al., 2013; Moore & Lockner, 2004; Scruggs & Tullis, 1998). Here, we consider the processes that determine gouge strength, noting that the relevant process should produce slip hardening that may closely approach but never reaches true steady state.

2.1. Microstructural Model

Inspired by the microstructures observed in sheared phyllosilicate gouges (Figure 1), we propose that frictional strength must be controlled by mechanical interactions or barriers operating at one or more of the following microstructural scales: (1) the polygranular clast or sigmoidal microlithon scale, (2) the phyllosilicate platelet or grain scale, (3) the grain surface ledge or cleavage step scale, and (4) the atomic scale—see Figure 1.

Experimental studies addressing phyllosilicate gouge friction describe the occurrence of localized, throughgoing shear bands, usually in the R_1 but also the P and Y orientations (e.g., Rutter et al., 1986). From detailed microstructural descriptions (Den Hartog et al., 2013; Van Diggelen et al., 2010) and images (Mariani et al., 2006; Moore & Lockner, 2004), the grain size in these bands appears predominantly submicron (note that Haines et al., 2013, measured a dominance of submicron particles for the entire sheared gouge). The sigmoidal or rhomb-shaped domains or clasts between the shear bands usually show coarser grained phyllosilicates (Den Hartog et al., 2013), often with intense kinking (Lu & He, 2014; Misra & Burg, 2012; Scruggs & Tullis, 1998; Van Diggelen et al., 2010). However, the shear strain that kinking can accommodate is limited. All this implies that shear bands accommodate most of the imposed shear deformation and that interactions at the submicron grain scale within them control frictional strength, rather than processes at the scale of the intervening sigmoidal domains or clasts (Figure 1). Due to the serial hence additive nature of these interactions (Interactions 2–4 above and in Figure 1), the strongest will control the macroscopic frictional behavior.

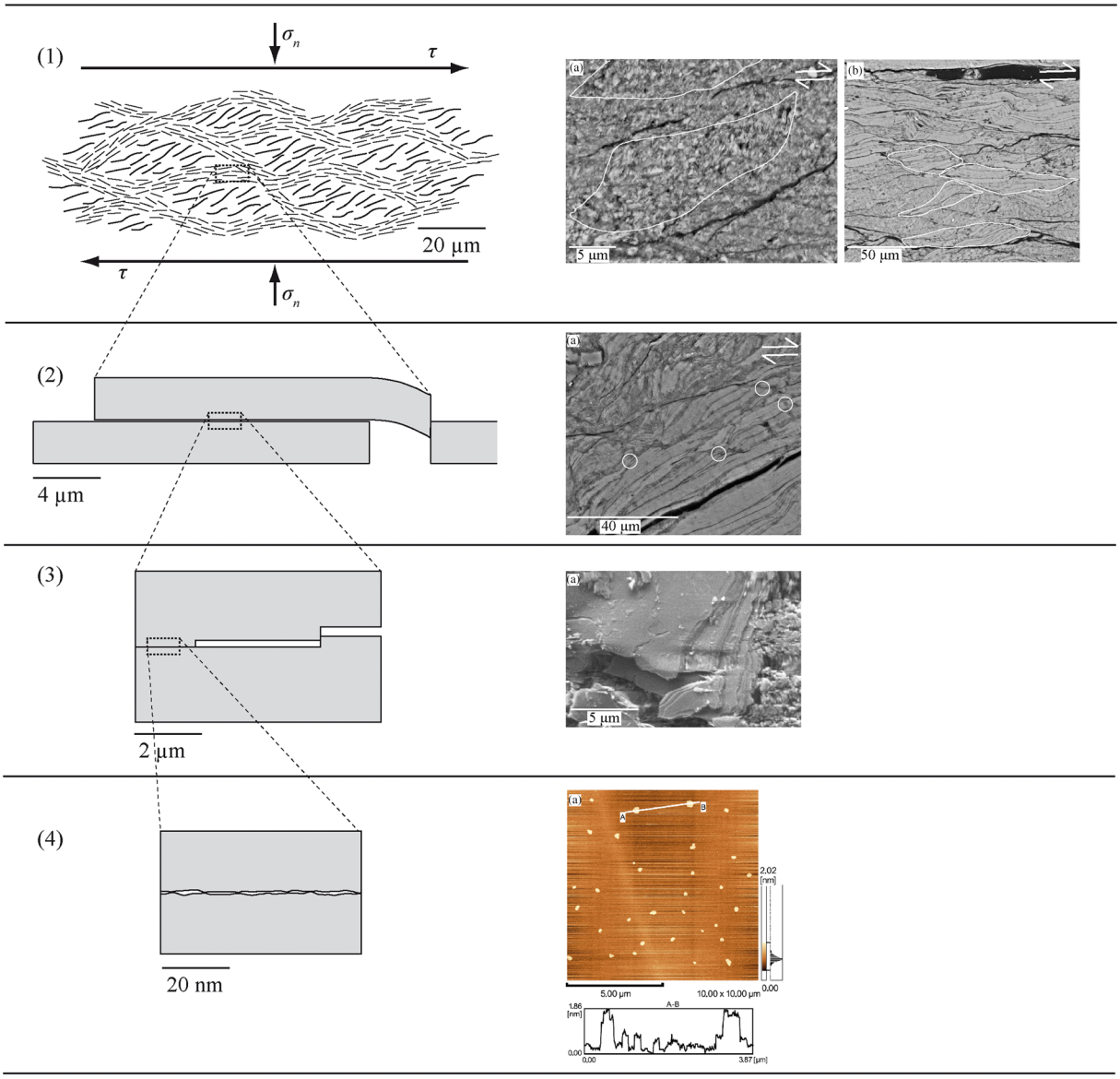

Figure 1. Scales of mechanical interactions or barriers that can control the frictional strength of phyllosilicates, schematically (left) and as observed for sheared gouges (right). (1) Polygranular clast or sigmoidal microlithon scale, (2) phyllosilicate platelet or grain scale, (3) grain surface ledge or cleavage step scale, and (4) atomic scale. Scale bars in the schematic figures are approximate. Micrographs are (1a) sample RSM3 of Den Hartog et al. (2013); (1b) and (2a) are samples bio-b05 and bioN01 of Lu and He (2014), respectively; (3a) is the phlogopite I sample of Moore and Lockner (2004); and (4) Figure 2a is an atomic force microscope image of a muscovite surface, taken from Kawai et al. (2015).

Observations on the internal, submicrometer grain structure of shear bands are rare. However, observations on coarser grained portions of sheared gouge provide insight into how platy grains interact mechanically (Figure 1). Frayed, folded, jagged and comminuted platelet tips (Figures 1 (2) and 1 (3)) suggest that bending, cleavage, and fragmentation (hence grain size reduction) occur at colliding grain edges as platelets slide over each other. We accordingly propose that the frictional strength of phyllosilicate gouges is controlled by the resistance to slip between platy grains provided by overlapping grain edges (Figure 1 (2)). Smaller scale cleavage ledges on the (001) grain surfaces (Figure 1 (3)) may provide similar (lower) resistance. Atomic scale shear resistance between (001) grain interfaces (e.g., due to Van Der Waals or other surface forces; see also Homola et al., 1990) operates in series with these edge and ledge interactions processes. Shear resistance on (001) interfaces will dominate phyllosilicate friction if the resistance provided by atomic scale shear resistance exceeds that of the overlapping grain edges. Measured friction coefficients of atomically flat (001)

Table 1
List of Experimentally Obtained Values of the Atomic Scale Friction Coefficient From the Literature

Friction coefficient	Material and conditions	Reference
0.008	Chlorite, σ_n = 300 MPa, P_f = 220 MPa, 300°C	Okamoto et al. (2019)
0.08	Muscovite, $\sigma_n \approx$ 50–170 MPa, P_f = 120 MPa, 600°C	Niemeijer (2018)
0.17	Muscovite, σ_n = 24 MPa, wet, room temperature	Kawai et al. (2015)
0.27	Muscovite, wet, room temperature	Homola et al. (1990)
0.28	Muscovite, σ_n = 24 MPa, room dry, room temperature	Kawai et al. (2015)
0.2–0.3	Muscovite, σ_n = 5–60 MPa, almost 0% RH, room temperature	Sakuma et al. (2018)
0.35	Muscovite, dry air, room temperature, normal load up to ~0.05 kN	Homola et al. (1990)

Note. All experiments were performed on single crystals of phyllosilicates.

phyllosilicate sheets ($\tilde{}\mu$) vary by orders of magnitude (Table 1), with $\tilde{}\mu$ of only 0.008 for single crystals of chlorite at a normal stress of 300 MPa, pore fluid pressure of 220 MPa, and 300°C (Okamoto et al., 2019) and $\tilde{}\mu$ as high as 0.35 in dry air at room temperature and very low normal loads (up to ~0.05 kN) (Homola et al., 1990).

On the basis of the above, in the proposed model, the strength of the aggregate is taken to be controlled by atomic scale frictional interactions on grain interfaces operating in series with the resistance to slip offered by overlapping (colliding) grain edges. Such serial behavior implies that both processes contribute additively to the total frictional strength. For a given sliding velocity, on an individual sliding plane, the velocity at which overlapping grain edges can be stripped away will be equal to the imposed value.

In constructing our model, we assume that the grain edge barrier strength is controlled by critical (dry) and subcritical (wet) "edge crack growth" or stress corrosion cracking (SCC), constrained to occur along basal cleavage planes of the phyllosilicate platelet grains (cf. Thouless et al., 1987). This mechanism bears an indirect resemblance to the recently proposed mechanism of phyllosilicate deformation via migration of so-called ripplocations where delamination of phyllosilicate layers occurs to release layer normal elastic strain (Aslin et al., 2019). We ignore the resistance offered by comminution or plastic bending of the cleaved-off basal slivers as the mechanical work needed to drive these processes is small (see Text S1 in the supporting information). To provide a microstructural model describing grain edge interactions as individual grain platelets slide over each other, we adopt the basic 2-D repetitive unit shown in Figure 2. Sliding is assumed to occur on a single (weakest) sliding surface, composed of a planar array of these units, located within a localized Y shear band. As in Figure 2, the grains are taken to have length a, width a, and thickness b measured normal to (001). Pores have width S, and the grain overlap has height c. S depends on the porosity Φ via $S = \Phi a/(1-\Phi)$. For the low porosities expected in highly localized shear bands in phyllosilicate gouge materials,

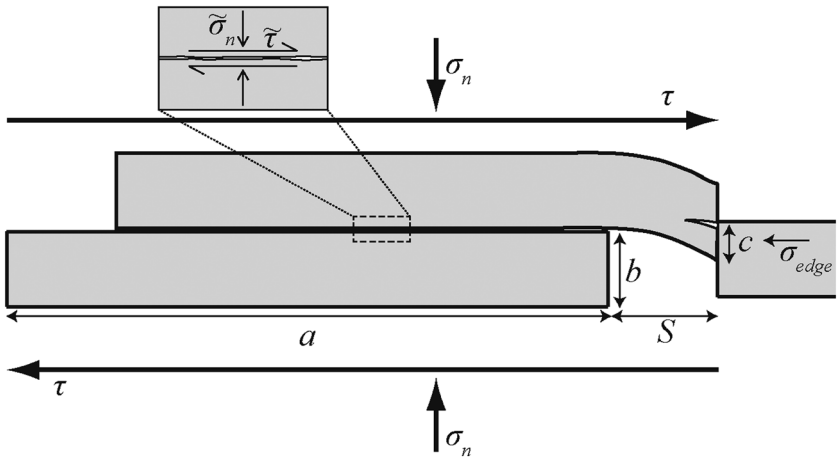

Figure 2. Model microstructure showing the main parameters used.

it is safe to assume that $S << a$. In this scenario, almost every overriding grain within a sliding surface is snagged at an edge barrier with a basal sheet being actively cleaved off from each grain as shear displacement proceeds.

2.2. Microphysical Formulation

We now derive a relationship for the macroscopic shear strength of pure phyllosilicate gouges, using the above assumptions and the model microstructure and definitions shown in Figure 2. Balancing macroscopic and local normal and shear forces acting within the microstructural unit, for displacements of the overriding grain of magnitude $\leq a$, we obtain: $\tilde{\sigma}_n(a-S)=\sigma_n(a+S)$ and $\tau(a+S)=\tilde{\tau}(a-S)+\sigma_{edge}c$. Combining these and defining the microscopic intergrain friction coefficient as $\tilde{\mu}=\tilde{\tau}/\tilde{\sigma}_n$ then yields

$$\tau=\tilde{\mu}\sigma_n+\frac{\sigma_{edge}c}{a+S} \text{ or } \mu=\tilde{\mu}+\frac{\sigma_{edge}c}{\sigma_n(a+S)} \tag{1}$$

for the corresponding macroscopic shear stress and friction coefficient μ of the phyllosilicate aggregate, where $\tilde{\tau}$ and $\tilde{\sigma}_n$ are the local shear and normal stresses, σ_n is the macroscopic (effective) normal stress, and σ_{edge} is the normal stress acting on the interacting grain edge contacts or barriers. The first and second terms on the right-hand side represent the shear resistance due to grain interface sliding and grain edge barriers, respectively. For further displacements up to a distance S beyond a (thus completing one full wavelength of displacement in Figure 2), the first term remains valid, but the second term falls to zero as the edge barrier has been removed (refer Figure 2). However, for the low porosities expected in a sliding surface composed of the microstructural units depicted in Figure 2, we have $S << a$ as discussed above, so that the loss of term 2 over the small distance S has only a minor effect on the average shear stress supported over a full wavelength of displacement of magnitude $(a + S)$ (Figure 2). The average sliding surface strength is therefore suitably approximated by Equation 1, especially noting that in reality the parameters a, S, and b will be distributed, so that when porosity and S are small, then, at any instant, almost every overriding grain will be snagged at an edge barrier.

Assuming normal compression of the aggregate under the action of the effective normal stress by linear elastic processes only, the grain overlap height c can now be obtained. This is done by approximating the ratio of c to the grain/platelet thickness b as being equal to the elastic strain ε_n produced by normal loading and by using the definition of the 1-D elastic compression modulus $E_a = \sigma_n/\varepsilon_n$, yielding

$$c \approx \frac{b\sigma_n}{E_a} \tag{2}$$

Following the analysis by Thouless et al. (1987) (or the simpler energy balance approach in Text S2), the stress intensity factor for an edge crack with the geometry shown in Figure 2 is given as

$$K=\beta\sigma_{edge}\sqrt{c} \tag{3}$$

where β is a geometric factor falling in the range 0.36–1.15, so approximately 1 (cf. KII of Thouless et al., 1987, without moment). If γ_{vac} is the specific surface energy in vacuum and E_{xtal} is the Young's modulus of the grain (e.g., Obreimoff, 1930), the Griffith criterion for critical edge crack growth is then

$$\beta\sigma_{edge}\sqrt{c} \leq \sqrt{2\gamma_{vac}E_{xtal}} \tag{4}$$

Using the definition of the mechanical energy release rate, $G = K^2/E_{xtal}$, we obtain from 4

$$G=\frac{\beta^2\sigma_{edge}^2 c}{E_{xtal}} \leq 2\gamma_{vac} \tag{5}$$

for critical crack extension. This gives the maximum resistance offered to cleaving-off grain edges as grains slide over each other. However, at lower shear stresses and hence σ_{edge} values, subcritical crack growth may occur at a velocity given by the classical theory of rate processes (Lawn, 1993; Wan, Aimard, et al., 1990; Wan, Lathabai, et al., 1990) as

$$V_{SCC}=2v_0a_0exp\left(\frac{-\Delta F}{kT}\right)sinh\left[\frac{\alpha_{SCC}(G-2\gamma_{env})}{kT}\right] \quad (6)$$

Here v_0 is a fundamental lattice vibration frequency; kT/h, with h being Planck's constant and k Boltzmann's constant; a_0 is a characteristic atomic spacing; ΔF is the activation energy for crack growth; α_{SCC} is an activation area; and γ_{env} is the cleavage surface interfacial energy in the environment supporting subcritical crack growth ($\gamma_{env} < \gamma_{vac}$). The intergranular sliding velocity V in the subcritical regime will be equal to V_{scc} as both sliding and cleavage occur in series and are both equal to the sliding velocity imposed on the assumed microstructural unit (Figure 2). Combining Equations 5 and 6 thus yields a relation between V and σ_{edge}, which can be solved to compute σ_{edge} as a function of V for different subcritical crack growth environments (e.g., different relative humidities) expressed through γ_{env} (see also Text S3).

3. Model Predictions and Comparison With Experimental Results

Model predictions were made for muscovite friction using Equation 1, assuming that sliding occurs at velocity V on a single near-planar set of grain interfaces, within a single shear band, at any instant (i.e., on the weakest planar sliding surface), solving for σ_{edge} as described above (see also Text S3), and using the parameter values given in the supporting information (Text S4). To capture the uncertainty in the value of the atomic scale resistance ($\tilde{\mu}$) to frictional sliding on atomically flat (001) interfaces, we made predictions for three values of this parameter: 0.01, 0.1, and 0.35. The lowest value is based on the value of 0.008 measured for (wet) chlorite single crystals by Okamoto et al. (2019), the intermediate value of 0.1 is close to the value of 0.08 measured by Niemeijer (2018) for (wet) muscovite single crystals, and 0.35 was measured for mica sheets at room temperature in dry air by Homola et al. (1990) and is the largest measured value to our knowledge (Table 1). Because of the large uncertainty in this parameter, we made no attempt to account for the effect of humidity on it. Therefore, predictions using the value of 0.35, obtained at dry conditions, are likely overestimations. Widely used experimental conditions were chosen as reference condition (25°C, σ_n of 100 MPa, V of 1 μm/s, and RH of 100%). Given the lack of quantitative measures of the grain size in shear bands, we use a reference grain size a of 250 nm and grain thickness of 37.5 nm, which is of similar aspect ratio (between 5:1 and 7:1) as observed by Den Hartog et al. (2013) for sigmoidal regions in muscovite gouges, but smaller as we are modeling the finer grained shear band. We assumed a porosity ϕ of 6% (as reported for 1 mm thick muscovite gouge sheared to 5 mm at 100 MPa effective normal stress by Zhang et al., 2001). The effects of grain size and porosity are discussed below. Muscovite is the only phyllosilicate for which subcritical crack growth data (i.e., parameters values in Equation 6) are available under dry, wet, and varying RH conditions, and we expect it to be representative of any common mica with a potassium interlayer. We accordingly compare our model results with experimental data on the frictional behavior of muscovite and other 2:1 sheet silicates that have a similar structure and bonding energy, that is, illite, paragonite, biotite (e.g., phlogopite), and chlorite (Moore & Lockner, 2004; Sakuma & Suehara, 2015). We do not include data on smectite clays because of (a) their much weaker interlayer bonding and (b) the swelling behavior they exhibit due to uptake of water and CO_2 into the interlayer region as a function of the chemical activity (or partial pressure) of these species (e.g., de Jong et al., 2014).

Figure 3 shows model predictions for μ as a function of RH for the reference conditions of temperature (25°C), normal stress (100 MPa), and sliding velocity (1 μm/s), along with example experimental data obtained at similar conditions—and a range of shear displacements (or shear strains γ_{strain}) encompassing the value of 5 mm ($\gamma_{strain} = 5$) upon which our choice of reference porosity of 6% is based (varied in Figure 3 from 3% to 9%, thus covering the maximum range we feel is likely for a localized slip surface or zone). Note that the experimental data do not show trends related to the type of sheet silicate. The dependence of our model predictions on the humidity are the result of the crack velocity parameters chosen, which were derived from new fits of Equation 6 to data by Wan, Aimard, et al. (1990) and Wan, Lathabai, et al. (1990) obtained at relative humidities of 3%, 5%, 20%, 60%, 90%, and 100% (see also Text S4, Figure S2, and Table S2). The coarse steps in these data cause the kink at 90% RH. The experimental data for all "dry" samples are plotted at RH of zero, as in no case was the water activity actually reported. However, without applying high vacuum and/or high temperature to the sample, under drained "in-apparatus" conditions before or during friction testing, sample chamber humidity is likely in the range of

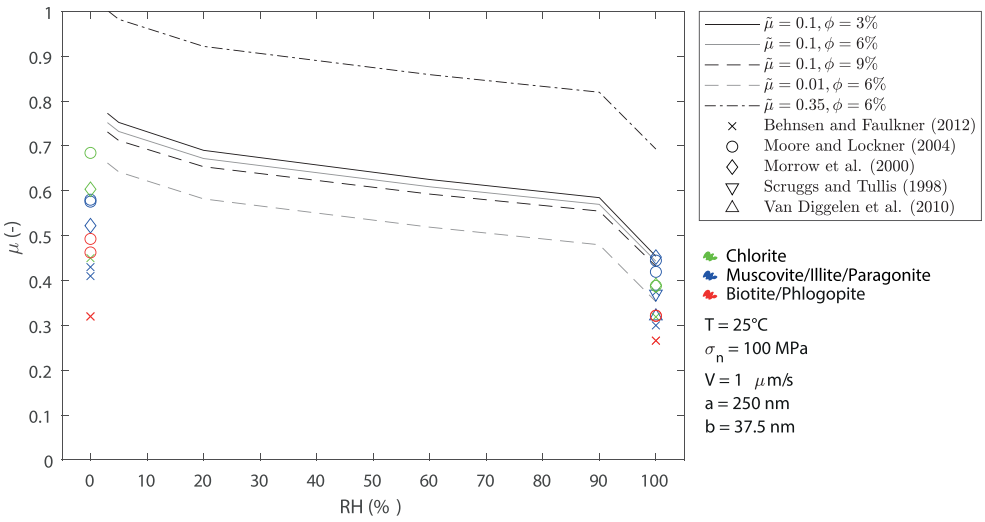

Figure 3. Friction coefficient versus relative humidity, showing model predictions (lines) and experimental data (symbols). The data of Behnsen and Faulkner (2012) are obtained at a slip velocity of 0.5 μm/s and a displacement of 1.4–1.6 mm (corresponding to $\gamma_{strain} \approx 1.5$ using an estimated initial sample thickness of ~1 mm). The data of Moore and Lockner (2004) and Morrow et al. (2000) are obtained at a slip velocity of 0.58 μm/s, at displacements of ~4.5 mm (dry) and ~10.3 mm (wet) (initial sample thickness ~1 mm, corresponding to γ_{strain} of 4.5 and 10.3). The data point at 100% RH of Scruggs and Tullis (1998) is obtained at a slip velocity of 1–10 μm/s, at steady state displacements of ~150 mm (initial sample thickness ~1 mm, corresponding to γ_{strain} of ~150). The data point of Van Diggelen et al. (2010) at 100% RH is obtained at a slip velocity of 1 μm/s and is the average of three steady-state intervals (initial sample thickness ~1 mm, $\gamma_{strain} < 37.7$). Color indicates different mineral groups. Note that paragonite was not measured individually but only mixed with muscovite, by Moore and Lockner (2004). The model predictions are made using the default conditions and parameter values given in the text and Table S1, employing porosities of 3%, 6%, and 9% to account for effects of varying shear displacement on porosity around the reference value of 6% reported by Zhang et al. (2001) for displacements of 5 mm (see the text). Values of 0.01, 0.1, and 0.35 are used for the atomic scale friction coefficient to account for the uncertainty in this parameter. For a detailed discussion, see the main text.

a few percent RH (carefully dried samples, such as those of Moore & Lockner, 2004) or possibly even a few tens of %. We have not included data obtained in studies in which the humidity was not controlled in some way or otherwise specified (Ikari et al., 2011; Shimamoto, 1986; Shimamoto & Logan, 1981), or where the slip velocity and displacement values are not given per friction value (Ikari et al., 2011). Despite the uncertainty in RH corresponding to the "dry" experimental data points, individual author-specific experimental data sets and our model predictions plotted in Figure 3 show a similar decrease in friction coefficient with increasing the RH. The predicted μ values at 100% RH fall within the range of experimental results obtained at these water-saturated conditions, except when $\tilde{\mu}$ is 0.35, which yields higher values than the experimental measurements. The predicted μ values for $\tilde{\mu}$ of 0.01 or 0.1 at 3% humidity are close to the single data point for dry chlorite obtained by Moore and Lockner (2004) but about 0.05–0.4 higher than the other experimental values. Similar to the result at 100% RH, the curve for the maximum $\tilde{\mu}$ value of 0.35 predicts friction coefficients about two times as high as observed in experiments. As the lower values used for $\tilde{\mu}$ are based on experiments performed wet, the model predictions at 3% RH are too high. This may be due to imperfect drying in the dry experiments. Alternatively, this difference may also be due to our selected grain size and porosity, both of which are known to decrease with increasing shear displacement during friction experiments (e.g., Den Hartog et al., 2013). Notably, the "dry" data presented by Moore and Lockner (2004) were derived at smaller displacements (~4.5 mm) than those of their wet data (~10.3 mm displacement); at low displacements, these gouges likely had larger grain sizes and porosities than gouges sheared to large displacements. Figure 4 shows contours of μ predicted by the model at the reference conditions in grain size versus porosity space. A reduction in grain size and in porosity, for typically observed grain aspect ratios (e.g., Den Hartog et al., 2013, or Figure 1), increases the number of grain edge interactions per unit area of sliding surface, resulting in a higher resistance exerted by the grain edges and accordingly an increase in the friction coefficient. Therefore, for the dry data of Moore and Lockner (2004), our selected reference grain size and porosity may have been too small, yielding too high a predicted friction coefficient. The slip hardening seen in virtually all experiments on the

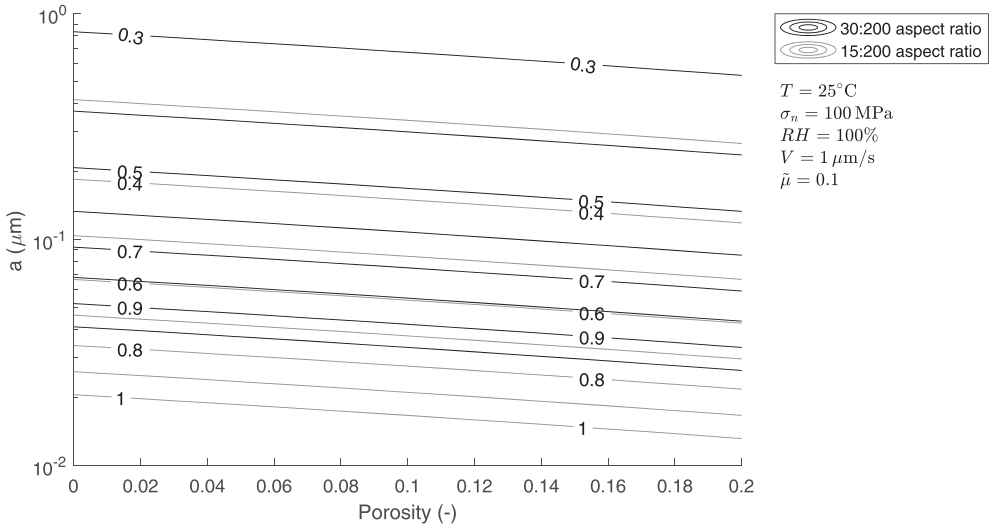

Figure 4. Contours of μ in porosity—grain size space for the aspect ratios as indicated, using the intermediate value for the atomic scale friction coefficient of 0.1.

phyllosilicates considered here may similarly be explained by ongoing grain size and porosity reduction. Consistent with these trends, our model implies that progressive cleavage and comminution of the cleavage flakes produced at colliding grain edges will lead to continuous grain size and porosity reduction (filling by fines) during shear of a phyllosilicate gouge. Figure 4 accordingly predicts an increase in friction coefficient from values below 0.3 in wet gouges with a grain size greater than 1 μm and porosity of say 20–25%, to 0.3–0.5 at 0.2–0.3 μm grain size and 10% porosity.

Model predictions for the effect of normal stress on the friction coefficient at 100% RH are shown in Figure 5, keeping all other parameters constant. The figure compares model predictions with experimental data obtained at similar conditions. The model predicts that the friction coefficient depends on the inverse

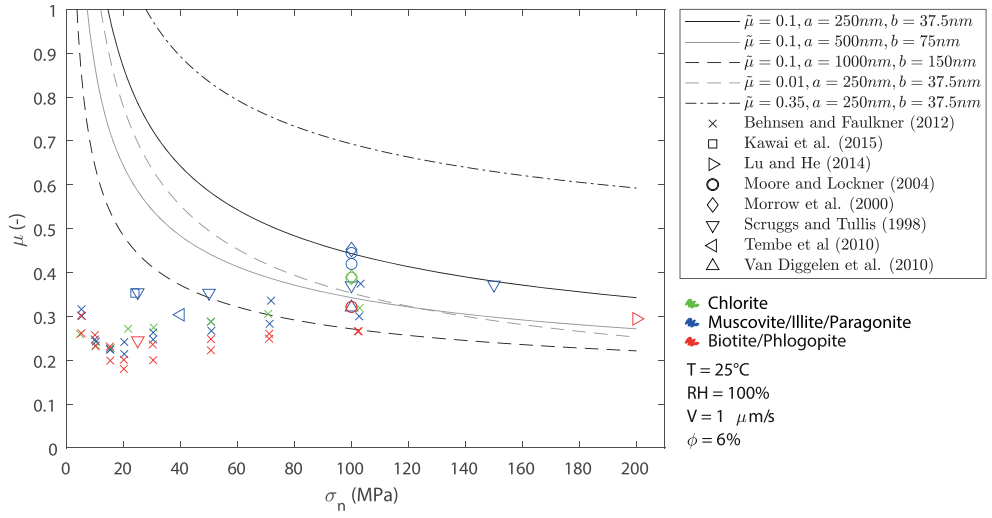

Figure 5. Friction coefficient versus normal stress, showing model predictions for different grain sizes and values of the atomic scale friction coefficient (lines) and experimental data (symbols). The experimental data by Lu and He (2014), Tembe et al. (2010), and Kawai et al. (2015) are obtained at slip velocities of 1.22, 1, and 3 μm/s and shear displacements of 3.2, 9.2, and ~5 mm, respectively. Given initial sample thicknesses of 1, 1, and 0.5 mm for these experiments, the data were obtained at shear strains of 3.2, 9.2, and 10, respectively. Shear strain for the data of Behnsen and Faulkner (2012) increases with normal stress from ~0.2 to 1.6 (using an estimated initial sample thickness of ~1 mm and the normal stress-stepping nature of the experiments). Data by Scruggs and Tullis (1998) are obtained at displacements of 6–331 mm (initial sample thickness ~1 mm, corresponding to γ_{strain} of 6–331). All other conditions are as reported in Figure 3.

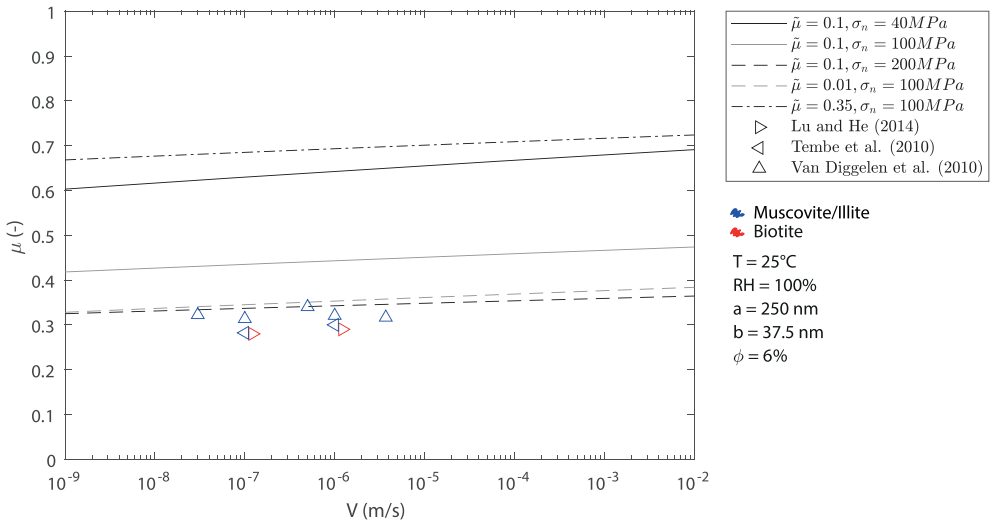

Figure 6. Friction coefficient versus slip velocity, showing model predictions for different values of the normal stress and atomic scale friction coefficients (lines) and experimental data (symbols). Data by Lu and He (2014) are obtained at displacements of 2.9 and 3.2 mm for velocities of 0.122 and 1.22 μm/s (initial sample thickness 1 mm, corresponding γ_{strain} of 2.9 and 3.2) while data by Tembe et al. (2010) are obtained at 6.9 and 9.2 mm for velocities of 0.1 and 1 μm/s (initial sample thickness 1 mm, corresponding γ_{strain} of 6.9 and 9.2). Data by Van Diggelen et al. (2010) are obtained in a single velocity-stepping experiment following the sequence 1, 3.7, 0.1, 1, 0.03, 1, and 0.5 μm/s, with total shear strain $\gamma_{strain} < 37.7$.

of the square root of the normal stress, which agrees poorly with the experimental data. The various discrepancies seen in Figure 5, especially the overprediction of friction coefficient at normal stress <20 MPa, may be the result of the effect of grain size and porosity on the friction coefficient (Figure 4), both of which are expected to increase with a decrease in normal stress (see Zhang et al., 2001, for porosity), which would yield a decrease in the predicted friction coefficient (Figure 4). Notably, Zhang et al. (2001) showed that the porosity in muscovite gouge sheared over a displacement of 5 mm is 6% at 100 MPa versus 14% at 25 MPa (i.e., a 125% increase). At our reference grain size (250 nm) and $\tilde{\mu}$ of 0.1, a porosity of 14% instead of 6% at 25 MPa yields an decrease in μ of 0.06. The effect of grain size is more significant so that, at 14% porosity, we would need a grain size of ~2 μm for our model predictions to match with the experimentally measured friction coefficient of around 0.3. The effect of grain size is illustrated in Figure 5 by curves for different grain sizes; however, we do not have any constraints on the change in grain size with normal stress. Alternatively, effects that have not been taken into account here on the frictional behavior of pure phyllosilicates may be important, notably at lower normal stresses. Figure 5 also emphasizes the need for better constraints on $\tilde{\mu}$ as the predicted friction coefficients are critically dependent on this parameter.

Finally, our model predicts a weak increase in the friction coefficient with slip velocity (Figure 6). This is consistent with the subtle velocity strengthening behavior of pure phyllosilicates at room temperature (e.g., Ikari et al., 2011), and with data of Lu and He (2014) and Tembe et al. (2010) in Figure 6 at sliding rates of 10^{-7} to 10^{-6} m s^{-1}. Van Diggelen et al. (2010) provided friction coefficients obtained in constant velocity experiments performed at a wider range of velocities (of order 10^{-8} to 10^{-5} m s^{-1}; Figure 6). However, variability of other parameters in those experiments obscures any weak velocity dependence of friction. Effects of slip velocity on the velocity dependence of friction, as reported by Ferri et al. (2011; see also Bar-Sinai et al., 2014) in lab-dry, clay-rich gouges at slip rates above 10^{-3} m s^{-1}, or as observed, for example, by Den Hartog et al. (2014) for wet illite gouge at 200–500°C, are not captured by the current model and presumably reflect the operation of different microscale processes.

4. Discussion and Conclusion

The microphysical model for the frictional behavior of phyllosilicates predicts a broad range of effects of RH and slip velocity on friction coefficient, but it does not reproduce the trend with normal stress and shows

critical dependency of the friction coefficient on the atomic scale friction coefficient. Some of the anomalous friction coefficients predicted by our model may be due to grain size and porosity variations. Effects of grain size and porosity also have implications for the evolution of the friction coefficient with shear displacement. Notably, our model implies that progressive grain size and porosity reduction during slip lead to an increase in the friction coefficient, that is, to strain hardening. This is consistent with experiments on gouge layers of 1–2 mm thickness, which generally show continuous slip hardening behavior at decreasing but still positive rate, at least when plotted at displacements of tens of mm (e.g., Den Hartog et al., 2013, 2014; Scruggs & Tullis, 1998; Van Diggelen et al., 2010). Such strain hardening behavior, together with the velocity strengthening behavior of phyllosilicates raises the question of why slip often is found to localize in phyllosilicate-rich horizons in fault zones. A possible explanation is offered by Figure 4, which shows that the thinning of a phyllosilicate grain—which inevitably accompanies our proposed subcritical platelet cleavage process—reduces the friction coefficient. Thus, subcritical cleavage will help localize deformation in the band in which this process is active. Such a dynamic thinning of the grains has not been incorporated in the current model and should be explored in future models. Note, however, that field evidence suggests that localization onto a principal slip surface in phyllosilicate gouge zones may be the result of seismic slip rather than the subseismic shear considered here. Localization is observed along the Punchbowl fault, and this exposed fault section is believed to have slipped seismically (Chester & Chester, 1998) while localization observed along the Carboneras fault zone appears to represent slow creep on a number of phyllosilicate-rich fault strands, limiting the nucleation of larger seismogenic events to localized fault planes (Faulkner et al., 2003).

Discrepancies between our model results and experimental data could, of course, reflect additional processes that have not been accounted for but which might be equally important. Clearly, accurate predictions with the current model require further experiments to determine the atomic scale friction coefficient as the predictions are critically dependent on this variable. Finally, we emphasize that the current study is limited to predictions made at room temperature and at rupture patch nucleation as opposed to seismic slip velocities. At elevated temperatures, sliding resistance due to bending of cleaving-off phyllosilicate slivers into intergranular pores (Figure 2) via plastic processes may need to be incorporated, if (serial) platelet cleavage becomes sufficiently easy, as may pervasive plastic shear of the phyllosilicate grains. At seismic slip rates, other processes not accounted for in our model may dominate. In addition, we have not taken into account pore fluid pressurization effects or effects of dilatancy here, which may, respectively, lead to additional weakening (Faulkner et al., 2018) or strengthening of gouge zones when liquid water is present.

Acknowledgments

We thank C. He, Y. Bernabe, A. Kronenberg, and an anonymous reviewer for their helpful feedback. We thank Z. Lu and D. Moore for providing their original micrographs and V. Krizek for his help optimizing the model codes. We thank J.A. Roholl for performing preliminary experiments and modeling on pure phyllosilicates. The model codes are stored at Mendeley Data (den Hartog, S. A. M.; Faulkner, D. R.; Spiers, C. J. (2020), "Model codes microphysical model for phyllosilicate frictional behaviour," Mendeley Data, v1; https://doi.org/10.17632/3ywyjvnw88.1). This project has received funding from the European Union's Horizon 2020 Research and Innovation Programme under the Marie Sklodowska-Curie Grant Agreement 658464. D. F. acknowledges NERC Grants NE/R017484/1 and NE/P002943/1.

References

Aslin, J., Mariani, E., Dawson, K., & Barsoum, M. W. (2019). Ripplocations provide a new mechanism for the deformation of phyllosilicates in the lithosphere. *Nature Communications*, *10*(1), 686. https://doi.org/10.1038/s41467-019-08587-2

Bar-Sinai, Y., Spatschek, R., Brener, E. A., & Bouchbinder, E. (2014). On the velocity-trengthening behavior of dry friction. *Journal of Geophysical Research: Solid Earth*, *119*, 1738–1748. https://doi.org/10.1002/2013jb010586

Behnsen, J., & Faulkner, D. R. (2012). The effect of mineralogy and effective normal stress on frictional strength of sheet silicates. *Journal of Structural Geology*, *42*, 49–61. https://doi.org/10.1016/j.jsg.2012.06.015

Bos, B., Peach, C. J., & Spiers, C. J. (2000). Frictional-viscous flow of simulated fault gouge caused by the combined effects of phyllosilicates and pressure solution. *Tectonophysics*, *327*(3-4), 173–194. https://doi.org/10.1016/S0040-1951(00)00168-2

Byerlee, J. (1978). Friction of rocks. *Pure and Applied Geophysics*, *116*(4), 615–626. https://doi.org/10.1007/bf00876528

Chen, J., & Spiers, C. J. (2016). Rate and state frictional and healing behavior of carbonate fault gouge explained using microphysical model. *Journal of Geophysical Research: Solid Earth*, *121*, 8642–8665. https://doi.org/10.1002/2016JB013470

Chester, F. M., & Chester, J. S. (1998). Ultracataclastic structure and friction processes of the Punchbowl fault, San Andreas system, California. *Tectonophysics*, *295*(1–2), 199–221. https://doi.org/10.1016/S0040-1951(98)00121-8

Collettini, C., Niemeijer, A., Viti, C., & Marone, C. (2009). Fault zone fabric and fault weakness. *Nature*, *462*(7275), 907–910. https://doi.org/10.1038/nature08585

Crawford, B. R., Faulkner, D. R., & Rutter, E. H. (2008). Strength, porosity, and permeability development during hydrostatic and shear loading of synthetic quartz-clay fault gouge. *Journal of Geophysical Research*, *113*, B03207. https://doi.org/10.1029/2006jb004634

de Jong, S. M., Spiers, C. J., & Busch, A. (2014). Development of swelling strain in smectite clays through exposure to carbon dioxide. *International Journal of Greenhouse Gas Control*, *24*, 149–161. https://doi.org/10.1016/j.ijggc.2014.03.010

Den Hartog, S. A. M., Niemeijer, A. R., & Spiers, C. J. (2012). New constraints on megathrust slip stability under subduction zone *P-T* conditions. *Earth and Planetary Science Letters*, *353-354*, 240–252. https://doi.org/10.1016/j.epsl.2012.08.022

Den Hartog, S. A. M., Niemeijer, A. R., & Spiers, C. J. (2013). Friction on subduction megathrust faults: Beyond the illite-muscovite transition. *Earth and Planetary Science Letters*, *373*, 8–19. https://doi.org/10.1016/j.epsl.2013.04.036

Den Hartog, S. A. M., Saffer, D. M., & Spiers, C. J. (2014). The roles of quartz and water in controlling unstable slip in phyllosilicate-rich megathrust fault gouges. *Earth, Planets and Space*, *66*, 78. https://doi.org/10.1186/1880-5981-66-78

Den Hartog, S. A. M., & Spiers, C. J. (2014). A microphysical model for fault gouge friction applied to subduction megathrusts. *Journal of Geophysical Research: Solid Earth*, *119*, 1510–1529. https://doi.org/10.1002/2013jb010580

den Hartog, S. A. M., Faulkner, D. R., & Spiers, C. J. (2020). Model codes microphysical model for phyllosilicate frictional behaviour. *Mendeley Data*, *1*, https://doi.org/10.17632/3ywyjvnw88.1

Dieterich, J., & Kilgore, B. (1994). Direct observation of frictional contacts: New insights for state-dependent properties. *Pure and Applied Geophysics*, *143*(1–3), 283–302. https://doi.org/10.1007/bf00874332

Dieterich, J. H. (1978). Time-dependent friction and the mechanics of stick-slip. *Pure and Applied Geophysics*, *116*(4-5), 790–806. https://doi.org/10.1007/BF00876539

Dieterich, J. H. (1979). Modeling of rock friction 1. Experimental results and constitutive equations. *Journal of Geophysical Research*, *84*(B5), 2161–2168. https://doi.org/10.1029/JB084iB05p02161

Faulkner, D. R., Lewis, A. C., & Rutter, E. H. (2003). On the internal structure and mechanics of large strike-slip fault zones: Field observations of the Carboneras fault in southeastern Spain. *Tectonophysics*, *367*(3), 235–251. https://doi.org/10.1016/S0040-1951(03)00134-3

Faulkner, D. R., Sanchez-Roa, C., Boulton, C., & den Hartog, S. A. M. (2018). Pore fluid pressure development in compacting fault gouge in theory, experiments, and nature. *Journal of Geophysical Research: Solid Earth*, *123*, 226–241. https://doi.org/10.1002/2017jb015130

Ferri, F., Di Toro, G., Hirose, T., Han, R., Noda, H., Shimamoto, T., et al. (2011). Low- to high-velocity frictional properties of the clay-rich gouges from the slipping zone of the 1963 Vaiont slide, northern Italy. *Journal of Geophysical Research*, *116*, B09208. https://doi.org/10.1029/2011jb008338

Haines, S. H., Kaproth, B., Marone, C., Saffer, D., & van der Pluijm, B. (2013). Shear zones in clay-rich fault gouge: A laboratory study of fabric development and evolution. *Journal of Structural Geology*, *51*, 206–225. https://doi.org/10.1016/j.jsg.2013.01.002

Holdsworth, R. E., van Diggelen, E. W. E., Spiers, C. J., de Bresser, J. H. P., Walker, R. J., & Bowen, L. (2011). Fault rocks from the SAFOD core samples: Implications for weakening at shallow depths along the San Andreas Fault, California. *Journal of Structural Geology*, *33*(2), 132–144. https://doi.org/10.1016/j.jsg.2010.11.010

Homola, A. M., Israelachvili, J. N., McGuiggan, P. M., & Gee, M. L. (1990). Fundamental experimental studies in tribology: The transition from "interfacial" friction of undamaged molecularly smooth surfaces to "normal" friction with wear. *Wear*, *136*(1), 65–83. https://doi.org/10.1016/0043-1648(90)90072-I

Ikari, M. J., Marone, C., & Saffer, D. M. (2011). On the relation between fault strength and frictional stability. *Geology*, *39*(1), 83–86. https://doi.org/10.1130/G31416.1

Kawai, K., Sakuma, H., Katayama, I., & Tamura, K. (2015). Frictional characteristics of single and polycrystalline muscovite and influence of fluid chemistry. *Journal of Geophysical Research: Solid Earth*, *120*, 6209–6218. https://doi.org/10.1002/2015jb012286

Lawn, B. R. (1993). *Fracture of brittle solids*, (Second ed.). New York, USA: Press Syndicate of the University of Cambridge.

Lu, Z., & He, C. (2014). Frictional behavior of simulated biotite fault gouge under hydrothermal conditions. *Tectonophysics*, *622*, 62–80. https://doi.org/10.1016/j.tecto.2014.03.002

Mares, V. M., & Kronenberg, A. K. (1993). Experimental deformation of muscovite. *Journal of Structural Geology*, *15*(9–10), 1061–1075. https://doi.org/10.1016/0191-8141(93)90156-5

Mariani, E., Brodie, K. H., & Rutter, E. H. (2006). Experimental deformation of muscovite shear zones at high temperatures under hydrothermal conditions and the strength of phyllosilicate-bearing faults in nature. *Journal of Structural Geology*, *28*(9), 1569–1587. https://doi.org/10.1016/j.jsg.2006.06.009

Misra, S., & Burg, J.-P. (2012). Mechanics of kink-bands during torsion deformation of muscovite aggregate. *Tectonophysics*, *548–549*, 22–33. https://doi.org/10.1016/j.tecto.2012.04.014

Moore, D. E., & Lockner, D. A. (2004). Crystallographic controls on the frictional behavior of dry and water-saturated sheet structure minerals. *Journal of Geophysical Research*, *109*, B03401. https://doi.org/10.1029/2003JB002582

Morrow, C. A., Moore, D. E., & Lockner, D. A. (2000). The effect of mineral bond strength and adsorbed water on fault gouge frictional strength. *Geophysical Research Letters*, *27*(6), 815–818. https://doi.org/10.1029/1999GL008401

Morrow, C. A., Moore, D. E., & Lockner, D. A. (2017). Frictional strength of wet and dry montmorillonite. *Journal of Geophysical Research: Solid Earth*, *122*, 3392–3409. https://doi.org/10.1002/2016jb013658

Niemeijer, A. R. (2018). Velocity-dependent slip weakening by the combined operation of pressure solution and foliation development. *Scientific Reports*, *8*(1), 4724. https://doi.org/10.1038/s41598-018-22889-3

Niemeijer, A. R., & Spiers, C. J. (2007). A microphysical model for strong velocity weakening in phyllosilicate-bearing fault gouges. *Journal of Geophysical Research*, *112*, B10405. https://doi.org/10.1029/2007JB005008

Obreimoff, J. W. (1930). The splitting strength of mica. *Proceedings of the Royal Society of London A: Mathematical, Physical and Engineering Sciences*, *127*(805), 290–297. https://doi.org/10.1098/rspa.1930.0058

Okamoto, A. S., Verberne, B. A., Niemeijer, A. R., Takahashi, M., Shimizu, I., Ueda, T., & Spiers, C. J. (2019). Frictional properties of simulated chlorite gouge at hydrothermal conditions: Implications for subduction megathrusts. *Journal of Geophysical Research: Solid Earth*, *124*, 4545–4565. https://doi.org/10.1029/2018jb017205

Ruina, A. (1983). Slip instability and state variable friction laws. *Journal of Geophysical Research*, *88*(B12), 10,359–10,370. https://doi.org/10.1029/JB088iB12p10359

Rutter, E. H., Maddock, R. H., Hall, S. H., & White, S. H. (1986). Comparative microstructures of natural and experimentally produced clay-bearing fault gouges. *Pure and Applied Geophysics*, *124*(1–2), 3–30. https://doi.org/10.1007/BF00875717

Sakuma, H. (2013). Adhesion energy between mica surfaces: Implications for the frictional coefficient under dry and wet conditions. *Journal of Geophysical Research: Solid Earth*, *118*, 6066–6075. https://doi.org/10.1002/2013jb010550

Sakuma, H., Kawai, K., Katayama, I., & Suehara, S. (2018). What is the origin of macroscopic friction? *Science Advances*, *4*, eaav2268. https://doi.org/10.1126/sciadv.aav2268

Sakuma, H., & Suehara, S. (2015). Interlayer bonding energy of layered minerals: Implication for the relationship with friction coefficient. *Journal of Geophysical Research: Solid Earth*, *120*, 2212–2219. https://doi.org/10.1002/2015jb011900

Scruggs, V. J., & Tullis, T. E. (1998). Correlation between velocity dependence of friction and strain localization in large displacement experiments on feldspar, muscovite and biotite gouge. *Tectonophysics*, *295*(1–2), 15–40. https://doi.org/10.1016/S0040-1951(98)00113-9

Shimamoto, T. (1986). Strengthening of phyllosilicate and gypsum gouges with increasing temperature: Effect of temperature or moisture elimination? *International Journal of Rock Mechanics and Mining Science and Geomechanics Abstracts*, *23*(6), 439–443. https://doi.org/10.1016/0148-9062(86)92309-0

Shimamoto, T., & Logan, J. M. (1981). Effects of simulated clay gouges on the sliding behavior of Tennessee sandstone. *Tectonophysics*, *75*(3-4), 243–255. https://doi.org/10.1016/0040-1951(81)90276-6

Tembe, S., Lockner, D. A., & Wong, T.-F. (2010). Effect of clay content and mineralogy on frictional sliding behavior of simulated gouges: Binary and ternary mixtures of quartz, illite and montmorillonite. *Journal of Geophysical Research*, *115*, B03416. https://doi.org/10.1029/2009JB006383

Thouless, M. D., Evans, A. G., Ashby, M. F., & Hutchinson, J. W. (1987). The edge cracking and spalling of brittle plates. *Acta Metallurgica*, *35*(6), 1333–1341. https://doi.org/10.1016/0001-6160(87)90015-0

Van Diggelen, E. W. E., De Bresser, J. H. P., Peach, C. J., & Spiers, C. J. (2010). High shear strain behaviour of synthetic muscovite fault gouges under hydrothermal conditions. *Journal of Structural Geology*, *32*(11), 1685–1700. https://doi.org/10.1016/j.jsg.2009.08.020

Wan, K.-T., Aimard, N., Lathabai, S., Horn, R. G., & Lawn, B. R. (1990). Interfacial energy states of moisture-exposed cracks in mica. *Journal of Materials Research*, *5*(1), 172–182. https://doi.org/10.1557/JMR.1990.0172

Wan, K.-T., Lathabai, S., & Lawn, B. R. (1990). Crack velocity functions and thresholds in brittle solids. *Journal of the European Ceramic Society*, *6*(4), 259–268. https://doi.org/10.1016/0955-2219(90)90053-I

Zhang, S., Tullis, T. E., & Scruggs, V. J. (2001). Implications of permeability and its anisotropy in a mica gouge for pore pressures in fault zones. *Tectonophysics*, *335*(1-2), 37–50. https://doi.org/10.1016/S0040-1951(01)00044-0